Supporting Information
Thermal Boundary Conductance Across Heteroepitaxial ZnO/GaN Interfaces: Assessment of the Phonon Gas Model

John T. Gaskins,[†] George Kotsonis,[‡] Ashutosh Giri,[¶] Shenghong Ju,[§,‖] Andrew Rohskopf,[⊥] Yekan Wang,[#] Tingyu Bai,[#] Edward Sachet,[‡] Christopher T. Shelton,[‡] Zeyu Liu,[@] Zhe Cheng,[⊥] Brian M. Foley,[⊥] Samuel Graham,[⊥,△] Tengfei Luo,[@,∇] Asegun Henry,[⊥,△,††] Mark S. Goorsky,[#] Junichiro Shiomi,[§,‖] Jon-Paul Maria,[‡] and Patrick E. Hopkins[*,¶,‡‡,¶¶]

†*Department of Mechanical and Aerospace Engineering, University of Virginia, Charlottesville, Virginia 22904, USA*

‡*Department of Materials Science and Engineering, North Carolina State University, Raleigh, North Carolina 27695, USA*

¶*Department of Mechanical and Aerospace Engineering, University of Virginia, Charlottesville, Virginia 22904, USA*

§*Department of Mechanical Engineering, The University of Tokyo, Bunkyo, Tokyo 113-8656, Japan*

‖*Center for Materials research by Information Integration, National Institute for Materials Science, 1-2-1 Sengen, Tsukuba, Ibaraki 305-0047, Japan*

⊥*George W. Woodruff School of Mechanical Engineering, Georgia Institute of Technology, Atlanta, Georgia 30332, USA*

#*Department of Materials Science and Engineering, University of California, Los Angeles, California 90095, United States*

@*Department of Aerospace and Mechanical Engineering, University of Notre Dame, Notre Dame, Indiana 46556, USA*

△*School of Materials Science and Engineering, Georgia Institute of Technology, Atlanta, Georgia 30332, USA*

∇*Center for Sustainable Energy of Notre Dame (ND Energy), University of Notre Dame, Notre Dame, Indiana 46556, USA*

††*Heat Lab, Georgia Institute of Technology, Atlanta, Georgia 30332, USA*

‡‡*Department of Materials Science and Engineering, University of Virginia, Charlottesville, Virginia 22904, USA*

¶¶*Department of Physics, University of Virginia, Charlottesville, Virginia 22904, USA*

E-mail: phopkins@virginia.edu

Film Growth and Microstructural Characterization

Ga-polar GaN was prepared on a [0001]-sapphire wafer by metal-organic vapor phase epitaxy, employing an AlN buffer layer.[1,2] ZnO thin films were grown heteroepitaxially on GaN by pulsed-laser deposition using a Coherent KrF excimer laser with an energy density of ~ 1 J cm^{-2}, pulse rate of 10 Hz, pulse width of 20 ns, target-substrate distance of 45 mm, substrate temperature of 600 C, and an O_2 pressure of 10 mTorr. Base pressures of less than 0.003 mTorr were achieved prior to O_2 introduction and subsequent deposition.

XRD was performed using a Panalytical Empyrean diffactometer. High resolution XRD (i.e. Figure 1a in main manuscript) employed a 2-bounce Ge hybrid monochromator incident optic and 0.18° parallel plate collimator with proportional Xe detector. Long-range XRD data for second orientation identification is presented in Fig. 1. These scans employed a Bragg-Brentano HD incident optic and a PIXcel^{3D} area detector (i.e. divergent beam geometry) to maximize the observed intensity from all out-of-plane orientations. XRR was performed using the monochromator and parallel plate collimator optics and curve fitting was performed using the Panalytical X'Pert Reflectivity software package. Film thicknesses determined by XRR fitting have an uncertainty of 1-2 nm; film thicknesses determined by selective etching and profilometry have an uncertainty of ∼5-10 nm. AFM was performed with an Asylum atomic force microscope, model MFP3D, with conical AFM tips.

The reciprocal space map measurements were performed using a Jordan Valley (Bruker) D1 with an incident beam mirror to produce a parallel beam. A Si (200) channel cut crystal was equipped to monochromatize the beam. The scattered beam optics included a Si (220) channel cut crystal. X-ray based reciprocal space maps (RSMs) reveal the relaxation state of the ZnO films. Figure 2 includes the $(20\underline{2}4)$ reciprocal lattice points (RELPs) for both GaN and ZnO on the 180 nm thick film. GaN is at (0,0); the lower left feature corresponds to ZnO. For comparison, fully relaxed (red circle) and perfectly commensurate (black circle) RELPs are also indicated on the map. The RSM indicates that the film is close to, but not fully relaxed. From the peak position of the ZnO RELP (black triangle), the extent of

relaxation can be quantified; the relaxation state is 92 percent for the 180 nm thick film.

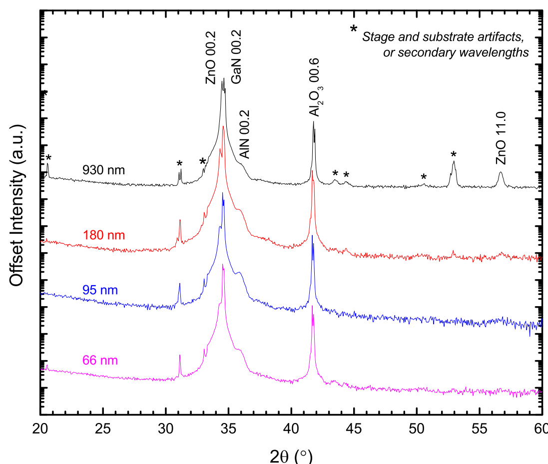

Figure 1: Offset XRD patterns for ZnO thin films of various thicknesses collected using Bragg-Brentano geometry to show the ZnO (002) reflection in thick samples. Film thicknesses are labeled on the left side of each trace and reflections are indexed. Reflections due to either substrate artifacts, stage reflections, or secondary wavelengths ($Cu_{\kappa\beta}$, W_L) are denoted with an asterisk.

The slight shift in 002 ZnO peak location as a function of thickness that can be seen in Figure 1a of the main text may be explained by epitaxial strain. The in-plane lattice mismatch between GaN (a = 3.19 Å; c = 5.19 Å) and ZnO (a = 3.25 Å; c = 5.21 Å) is ∼2%, which would correspond to a peak shift to lower 2θ of up to ∼0.8° for a perfectly commensurate film; calculated using a poisson's ratio of 0.364 for ZnO[3] and a simple biaxial strain model. We do not see such a pronounced shift (meaning the films are not perfectly commensurate), but it is reasonable to assume that the thinner films are under some amount of compressive in-plane strain, while thicker films relax toward the bulk c lattice parameter of ZnO.

The TEM samples were prepared using an FEI Nova 600 dual-beam focused ion beam tool and measurements were performed using an FEI Titan 300 kV electron microscope in the UCLA California NanoSystems Institute. Figure 3 includes Fourier transform filtered regions from the HRTEM image using the $(000l)$ reciprocal lattice points. The GaN (3a)

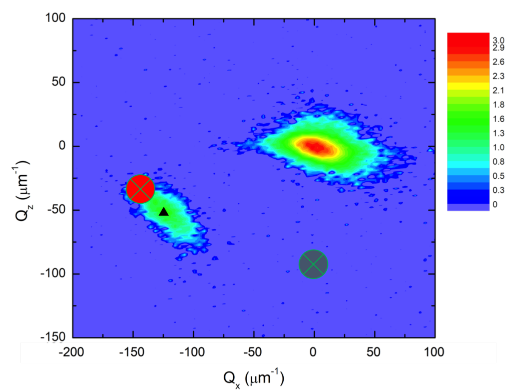

Figure 2: Reciprocal space map around the GaN $(20\underline{2}4)$ peak showing fully relaxed (red marker), fully strained (gray marker), and 92 percent relaxation for the 180 nm thick ZnO sample (black triangle).

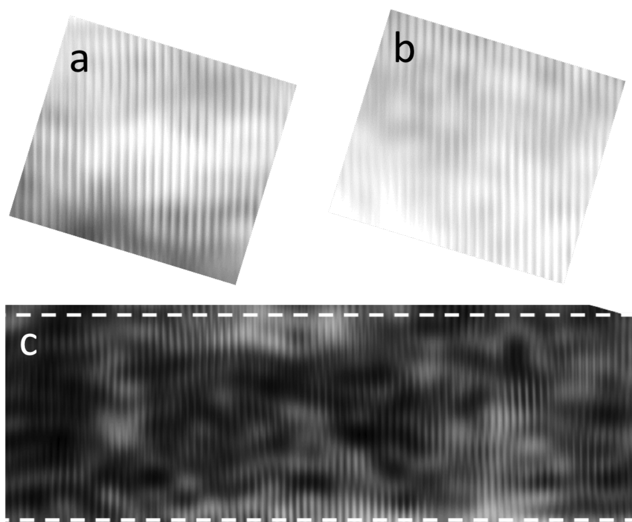

Figure 3: Filtered (0001) HRTEM images for (a) GaN, (b) ZnO, and (c) the 10 nm interfacial region.

and the ZnO (3b) away from the interface are distortion-free, whereas the 10 nm interfacial region (3c) shows distorted atomic planes.

Thin film TBC

As a further check to the validity of these TBC values found for the 180 and 95 nm films, we turn to a series of thin films with thicknesses of 5, 10, 19, 27, 42, and 66 nm. In this case we prescribe the thermal conductivity of ZnO from the analyses performed in the main manuscript and manually vary $h_{\mathrm{K,ZnO/GaN}}$ while fitting $h_{\mathrm{K,Al/ZnO}}$ and κ_{GaN}. We vary $h_{\mathrm{K,ZnO/GaN}}$ until the fitted value for κ_{GaN} is equal to the outer bound of the fitted thermal conductivity value for GaN from the control sample, in this case κ_{GaN} = 171 W m^{-1} K^{-1}. This value, averaged over all of the tests for the thin film samples, of $h_{\mathrm{K,ZnO/GaN}}$ = $380 \pm 65 MWm^{-2}$ K^{-1} represents the lower bound to the thermal boundary conductance at the ZnO/GaN interface. It is of note that this value is directly in line with the measured value of $h_{\mathrm{K,ZnO/GaN}}$ from the moderate thickness films. We acknowledge that in this case the conductance offered by the ZnO and the interface between the ZnO and GaN is seen as a lumped conductance in our thermal model where a change to either of these values would cause a proportional change to the other parameter. It is for this reason that we ignore the possibility of size effects in the thermal conductivity of the ZnO layer, which has recently been shown computationally,[4] since a reduction in the thermal conductivity of the ZnO layer would subsequently require an increase in $h_{\mathrm{K,ZnO/GaN}}$. This offers an even stronger case that the true lower bound to the thermal boundary conductance at the ZnO/GaN interface is $> 400 MWm^{-2}$ K^{-1}. It should be noted that attempting to reach the lower bound of the fitted GaN thermal conductivity by forcing the ZnO/GaN conductance higher results, in most cases, in nearly infinite conductances, which are unphysical.

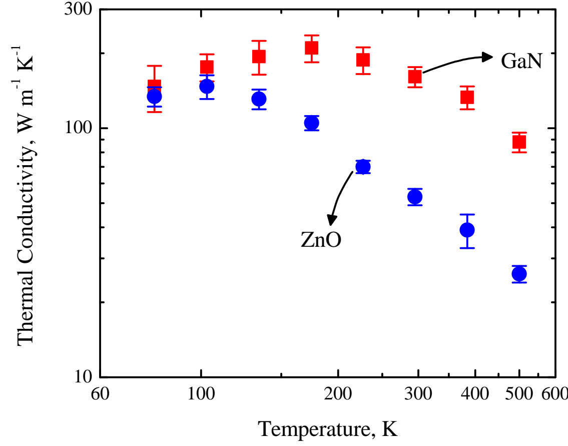

Figure 4: Temperature dependent thermal conductivity data for ZnO and GaN used in this study.

ZnO and GaN Temperature Dependent Properties

Figure 4 shows the thermal conductivity temperature trends for the 1.27 micron GaN on sapphire film and the 930nm ZnO on GaN on sapphire samples. While recent simulations of the thermal conductivity of ZnO and GaN[4] show higher values across the temperature range in question, we chose to use the measured value of thermal conductivity from the 930nm thick sample for all of our TBC calculations as they represent the measured values for the materials on which the ZnO films were grown.

Calculation of Contour Plots

The best fit values are determined by minimizing the sum of standard deviation between the model prediction and the TDTR data,

$$\sigma = \frac{\Sigma_{i=1}^{n}\left(\frac{r_{m,i}-rd,i}{r_{d,i}}\right)^2}{n} \tag{1}$$

, where n is the total number of time delays, and $r_{m,i}$ and $r_{d,i}$ are the ratios from the model

prediction and TDTR data, respectively. The lowest value of the contour lines corresponds to a 95% confidence interval, which indicates the combination of the respective variables with a deviation that is twice σ_{min}.

First Principles Lattice Dynamics Calculations of ZnO Thermal Conductivity

In an effort to examine whether this assumption is fully valid across the entire temperature range, we obtain the temperature dependent thermal conductivities in the same manner as calculated in Wu et. al. for the (001) direction. The bulk temperature dependent thermal conductivity of ZnO is computed by solving the phonon Boltzmann Equation iteratively by using first-principles force constants calculated from Quantum Espresso[5] via ShengBTE.[6] Local density approximation (LDA)[7] pseudopotential is applied in the first-principles calculation with a planewave cut-off of 50 Rydberg. The lattice structure is fully optimized to remove strain in the cell. The first Brillouin Zone is discretized as 16 x 16 x 16 in the Monkhorst-Pack scheme[8] for the Fermi's Golden rule calculation in the BTE solver for various temperatures. The mean free path accumulation for (0001) oriented ZnO is shown in fig. 5. We make note that the 930 nm thick film agrees well with the calculated thermal conductivity via FPLD.

DMM assumptions

In the limit of elastic scattering, applying the detailed balance to the phonon flux approaching the interface, the transmission coefficient from side 1 to 2 is given as,[9]

$$\zeta^{1\to 2}(k_1) = \frac{\sum_j k_{j,2}^2}{\sum_j k_{j,2}^2 + \sum_j k_{j,1}^2} \tag{2}$$

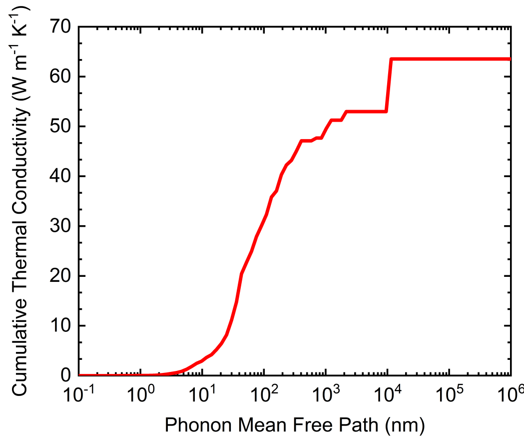

Figure 5: Mean free path accumulation for (0001) oriented ZnO.

Assuming crystallographic isotropy, we use Eq. 1 from the main manuscript with ζ calculated with Eq. 2 to predict the DMM-based TBC across ZnO/GaN interface. To this end, we use third order polynomial fits (where the phonon frequencies are given as $\omega(k)=Ak^3+Bk^2+Ck+D$) to the phonon dispersion relations in the $\Gamma \rightarrow$ M directions[10,11] and estimate the wave vector at the edge of the Brillouin Zone as $\pi/V^{1/3}$, where V is the calculated equilibrium volume at zero pressure.[10] The values of D in the polynomials for the longitudinal and transverse branches agree well with the corresponding sound velocities in the respective materials. Along with the sound velocities, the predicted heat capacities using these full dispersions agree very well with literature values of heat capacities for ZnO and GaN.[12,13] We compare these calculations to the more commonly used Debye approximation to the DMM where the dispersion is given by a single branch with a constant slope. The maximum phonon frequency in the Debye model is approximated as $\omega_{\mathrm{D}} = k_{\mathrm{B}}\theta_{\mathrm{D}}/\hbar$, where θ_{D} is the Debye temperature of the solid. The transmission coefficient is given by,

$$\zeta^{1\rightarrow 2} = \frac{v_{g,1}^{-2}}{v_{g,1}^{-2} + v_{g,2}^{-2}} \tag{3}$$

Figure 6a shows the predictions of Eq. 4 as a function of temperature for a ZnO/GaN interface considering both the more widely used Debye approximation and using a more

realistic dispersion relation for the following expression

$$h_{\mathrm{K}} = \frac{1}{4} \sum_{j} \int_{\mathbf{k}} C_j\left(\mathbf{k}\right) v_{g,j}\left(\mathbf{k}\right) \zeta\left(\mathbf{k}\right) d\mathbf{k} \tag{4}$$

The Debye approximation for a ZnO/GaN interface predicts agreeable conductances compared to using the full dispersion relations as shown in Fig. 6a. This is due to the fact that the over-prediction of the acoustic phonon frequencies and group velocities in the Brillouin zone is compensated for by its lack of not accounting for the optical phonons, which can significantly alter heat transport in these materials. Although the DMM predictions agree well with each other, they under-predict the measured TBC values by almost three fold. The fact that the DMM is more apt to predict diffuse scattering at non ideal interfaces suggests that the model is not appropriate for the high quality interfaces with minimal lattice mismatch of the epitaxial ZnO/GaN interfaces. As pointed out earlier, the measured values of the ZnO/GaN TBC are closer to the maximum conductances predicted compared to the predictions from the DMM, which further demonstrates the failure of DMM in correctly predicting conductances across high quality interfaces.

To further emphasize the importance of accurate modeling of interfacial transport, we analyze a GaN/diamond interface using the DMM, which is of great technological importance for GaN HEMTs. Figure 6b shows the predictions of Eq. 4 as a function of temperature for a GaN/diamond interface considering both the more widely used Debye approximation and using a more realistic dispersion relation for GaN and diamond (taken from Ref.[14]). Contrary to the ZnO/GaN interface, the DMM predictions with the Debye approximation for GaN/diamond greatly over-predicts the TBC as compared to the values predicted using the full dispersion. This can be attributed to the fact that the Debye model incorrectly approximates high group velocities for the phonon energies near the Brillouin zone edge and therefore predicts a much larger phonon flux approaching the interface. At room temperature, the Debye approximation for GaN/diamond interface predicts a TBR of $\sim$3 m^{-2} K^{-1}

GW, a value much lower than that predicted by using a realistic phonon dispersion, ∼10 m^{-2} K^{-1} GW, and is incorrectly used as a metric for designing GaN/diamond interfaces. These calculations further demonstrate the importance of judicious choice of phonon dispersions, as well as their use in an appropriate model, in order to accurately model and predict interface conductance at technologically relevant interfaces.

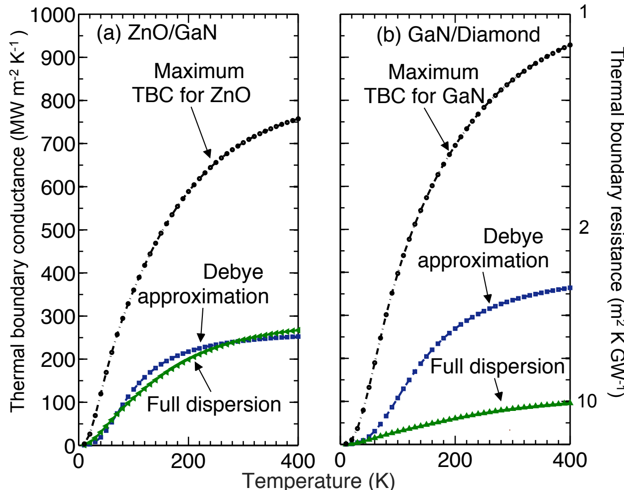

Figure 6: Comparisons of predictions for TBC using Eq. 4 with the DMM under the Debye approximation and using a realistic phonon dispersion for (a) ZnO/GaN interface and (b) GaN/diamond interface. The maximum conductances as predicted by Eq. 4 with ζ=1 are also included for comparison.

AGF assumptions

We investigated the phonon transmission and thermal conductance across a ZnO/GaN interface using the atomistic Green's function (AGF) method with second order force constants derived from first-principles calculations. The system for AGF calculations shown in Fig. 4 (a) is composed of three parts: ZnO leads, GaN leads, and the center device including the ZnO/GaN interface. In order to obtain the force constants for leads and interfacial parts based on the real-space displacement method[15,16] we adopted cuboid supercell structures with 128 atoms as shown in Fig. 4 (b) for density-functional theory (DFT) calculations.

The detailed calculations were performed using Quantum ESPRESSO[5] and ALAMODE[17] packages. The revised Perdew-Burke-Ernzerhof exchange-correlation functions based on generalized gradient approximation (GGA) was used and we considered 60 Ry plane-wave cutoffs for wave functions and 400 Ry kinetic energy cutoffs for charge density and potential. The obtained phonon dispersions of GaN and ZnO along high symmetry lines shown in Fig. 4 (c) and (d) agree well with previous experimental results[11,18].

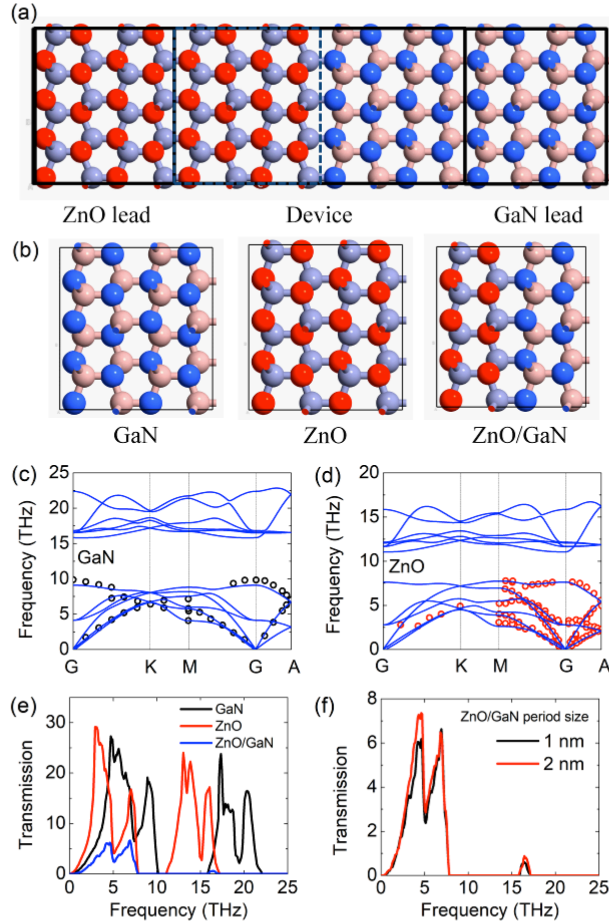

Figure 7: (a) System for AGF calculation. (b) Supercells for DFT calculations to obtain the force constants for GaN, ZnO, and the ZnO/GaN interface. (c)-(d) Calculated phonon dispersions for GaN and ZnO compared with experimental results. (e) Phonon transmission functions for pure GaN, ZnO, and the GaN/ZnO interface. (f) Comparison of interfacial phonon transmission with different super lattice period length.

In order to get accurate force constants for interfacial interactions, we separately extract the second order force constants associated with the atoms around the interface by repeating

the calculations for increasingly larger super lattice periods. As the period increased, the second order force constants for the atoms in the middle of each layer began to converge toward the bulk values. As a result, the second order force constants for the atoms away from the interface were interpolated between the super lattice and bulk values, while the values for the atoms located at the interface were taken from extrapolation of the increasing super lattice period values. In this way, the AGF super cell were constructed entirely from interpolated/extrapolated ab initio inputs. Figure 4 (e) shows the phonon transmission functions for pure GaN, ZnO, and the ZnO/GaN interface. For comparison, we tried two different super lattice periods of one and two nanometers for the interfacial force constant calculations. The difference of obtained transmission functions, shown in Fig. 4 (f), is small, which indicates that the interfacial interaction in our calculation is almost converged. The final value for interfacial thermal conductance reported in this work was modified by the four-probe method[19] which excludes the effect of leads and is nominally the same interfacial thermal conductance measured by the experiments.

References

(1) Collazo, R.; Mita, S.; Aleksov, A.; Schlesser, R.; Sitar, Z. Growth of Ga-and N-polar Gallium Nitride Layers by Metalorganic Vapor Phase Epitaxy on Sapphire Wafers. *Journal of crystal growth* **2006**, *287*, 586–590.

(2) Mita, S.; Collazo, R.; Rice, A.; Dalmau, R.; Sitar, Z. Influence of Gallium Supersaturation on the Properties of GaN Grown by Metalorganic Chemical Vapor Deposition. *Journal of Applied Physics* **2008**, *104*, 013521.

(3) Gadzhiev, G. G. The Thermal and Elastic Properties of Zinc Oxide-based Ceramics at High Temperatures. *High temperature* **2003**, *41*, 778–782.

(4) Wu, X.; Lee, J.; Varshney, V.; Wohlwend, J. L.; Roy, A. K.; Luo, T. Thermal Conduc-

tivity of Wurtzite Zinc-oxide from First-principles Lattice Dynamics - a Comparative Study with Gallium Nitride. *Scientific reports* **2016**, *6*.

(5) Giannozzi, P.; Baroni, S.; Bonini, N.; Calandra, M.; Car, R.; Cavazzoni, C.; Ceresoli, D.; Chiarotti, G. L.; Cococcioni, M.; Dabo, I. QUANTUM ESPRESSO: a Modular and Open-source Software Project for Quantum Simulations of Materials. *Journal of physics: Condensed matter* **2009**, *21*, 395502.

(6) Li, W.; Carrete, J.; Katcho, N. A.; Mingo, N. ShengBTE: A Solver of the Boltzmann Transport Equation for Phonons. *Computer Physics Communications* **2014**, *185*, 1747–1758.

(7) Perdew, J. P.; Zunger, A. Self-interaction Correction to Density-functional Approximations for Many-electron Systems. *Physical Review B* **1981**, *23*, 5048.

(8) Monkhorst, H. J.; Pack, J. D. Special Points for Brillouin-zone Integrations. *Physical review B* **1976**, *13*, 5188.

(9) Duda, J. C.; Beechem, T. E.; Smoyer, J. L.; Norris, P. M.; Hopkins, P. E. Role of Dispersion on Phononic Thermal Boundary Conductance. *Journal of Applied Physics* **2010**, *108*, 073515.

(10) Serrano, J.; Manjón, F.; Romero, A.; Ivanov, A.; Cardona, M.; Lauck, R.; Bosak, A.; Krisch, M. Phonon Dispersion Relations of Zinc Oxide: Inelastic Neutron Scattering and Ab Initio Calculations. *Physical Review B* **2010**, *81*, 174304.

(11) Ruf, T.; Serrano, J.; Cardona, M.; Pavone, P.; Pabst, M.; Krisch, M.; D'astuto, M.; Suski, T.; Grzegory, I.; Leszczynski, M. Phonon Dispersion Curves in Wurtzite-Structure GaN Determined by Inelastic X-ray Scattering. *Physical review letters* **2001**, *86*, 906.

(12) Kremer, R.; Cardona, M.; Schmitt, E.; Blumm, J.; Estreicher, S.; Sanati, M.; Bockowski, M.; Grzegory, I.; Suski, T.; Jezowski, A. Heat Capacity of α-GaN: Isotope Effects. *Physical Review B* **2005**, *72*, 075209.

(13) Touloukian, Y. S. *Thermophysical Properties of Matter: the TPRC Data Series; a Comprehensive Compilation of Data*; Ifi/Plenum, 1970; Vol. 1.

(14) Weber, W. Adiabatic Bond Charge Model for the Phonons in Diamond, Si, Ge, and α-Sn. *Physical Review B* **1977**, *15*, 4789.

(15) Esfarjani, K.; Chen, G.; Stokes, H. T. Heat Transport in Silicon from First-principles Calculations. *Physical Review B* **2011**, *84*, 085204.

(16) Esfarjani, K.; Stokes, H. T. Method to Extract Anharmonic Force Constants from First Principles Calculations. *Physical Review B* **2008**, *77*, 144112.

(17) Tadano, T.; Gohda, Y.; Tsuneyuki, S. Anharmonic Force Constants Extracted from First-principles Molecular Dynamics: Applications to Heat Transfer Simulations. *Journal of Physics: Condensed Matter* **2014**, *26*, 225402.

(18) Calzolari, A.; Nardelli, M. B. Dielectric Properties and Raman Spectra of ZnO from a First Principles Finite-differences/Finite-fields Approach. *Scientific reports* **2013**, *3*, 2999.

(19) Tian, Z.; Esfarjani, K.; Chen, G. Enhancing Phonon Transmission Across a Si/Ge Interface by Atomic Roughness: First-principles Study with the Green's Function Method. *Physical Review B* **2012**, *86*, 235304.